

# Hole-Mask Colloidal Nanolithography for Large-Area Low-Cost Metamaterials and Antenna-Assisted Surface-Enhanced Infrared Absorption Substrates

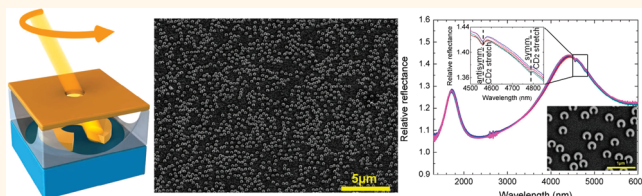
Stefano Cataldo,<sup>†,‡</sup> Jun Zhao,<sup>†,‡,\*</sup> Frank Neubrech,<sup>‡</sup> Bettina Frank,<sup>†</sup> Chunjie Zhang,<sup>§</sup> Paul V. Braun,<sup>§</sup> and Harald Giessen<sup>†</sup>

<sup>†</sup>4. Physics Institute and Research Center SCoPE, Pfaffenwaldring 57, University of Stuttgart, 70569 Stuttgart, Germany, <sup>‡</sup>Kirchhoff Institute for Physics, University of Heidelberg, Im Neuenheimer Feld 227, 69120 Heidelberg, Germany, and <sup>§</sup>Department of Materials Science and Engineering, University of Illinois at Urbana—Champaign, Urbana, Illinois 61801, United States. <sup>†,‡</sup>These authors contributed equally to this work.

Infrared spectroscopy is an important analytical tool for chemistry, biology, pharmacy, and medicine. Dipole- and Raman-active modes provide key information about structural and conformational properties of small molecular species as well as larger units, such as proteins or peptides. Unfortunately, the absorption and scattering cross-sections of molecules in the infrared are relatively low, which requires large quantities for analysis. One way to overcome this problem is the use of surface enhanced methods, such as surface-enhanced Raman spectroscopy (SERS) and surface enhanced infrared absorption spectroscopy (SEIRA). In these cases, the local electric field is strongly enhanced by plasmonic effects at rough metal surfaces, and hence, the lower detection limit is reduced.

Recently, resonantly enhanced SERS and SEIRA methods have been introduced.<sup>1–4</sup> Halas and co-workers introduced a nanoshell-covered large-area substrate that gives simultaneous SERS and SEIRA enhancement.<sup>5,6</sup> They demonstrate picomolar sensitivity and a 20000-fold SEIRA enhancement in comparison to common infrared absorption techniques. The SEIRA sensitivity was even further increased to the attomolar level by Neubrech *et al.*<sup>7</sup> using specifically tailored resonant nanoantennas. In particular, the detection of a monomolecular layer of octadecanethiol (ODT) was demonstrated using a simple Fourier-transform microscope and light from a synchrotron. Cubukcu *et al.*<sup>8</sup> and Pryce *et al.*<sup>9</sup> as well as

## ABSTRACT



We use low-cost hole-mask colloidal nanolithography to manufacture large-area resonant split-ring metamaterials and measure their infrared optical properties. This novel substrate is employed for antenna-assisted surface-enhanced infrared absorption measurements using octadecanethiol (ODT) and deuterated ODT, which demonstrates easy adjustability of our material to vibrational modes. Our method has the potential to make resonant plasmon-enhanced infrared spectroscopy a standard lab tool in biology, pharmacology, and medicine.

**KEYWORDS:** hole-mask colloidal nanolithography · large-area low-cost metamaterials · antenna-enhanced SEIRA substrate

Lahiri *et al.*<sup>10,11</sup> utilized metamaterial geometries for SEIRA, however on small-area samples fabricated by e-beam lithography. To bring these advances into biology and chemistry laboratories and allow for a plethora of applications, large-area low-cost fabrication is required.

Here we present an elegant solution to this problem by introducing a low-cost simple fabrication method for resonant nanoantenna SEIRA substrates with cm<sup>2</sup> of defect-free areas which allow for easy adjustment to the desired vibrational frequencies. We manufacture metallic split-ring-resonator (SRR) metamaterial nanoantennas using hole-mask colloidal nanolithography

\* Address correspondence to j.zhao@physik.uni-stuttgart.de.

Received for review December 8, 2011 and accepted December 16, 2011.

Published online  
10.1021/nn204798Z

© XXXX American Chemical Society

followed by tilted angle metal evaporation. We produced several samples with different SRR geometries and hence a set of different resonance frequencies to demonstrate easy adjustability. SEIRA sensing down to the monolayer sensitivity was observed for normal as well as deuterated (d-) ODT. At the same time, our manufacturing method represents an elegant method to produce large-area and low-cost SRR metamaterials with resonances in the near- and mid-infrared spectral range.

We are going to explain how to manufacture the hole-mask and the tilted-angle metal evaporation, followed by the optical characterization of the resonant SRR nanoantenna metamaterials, and demonstrate SEIRA sensing in two different vibrational frequency ranges with large sensitivity enhancement.

## RESULTS AND DISCUSSION

The hole-mask fabrication is depicted in Figure 1a–d, which is based on a similar method as that introduced by Fredriksson and co-workers.<sup>12</sup> We spin coat a PMMA layer with thickness  $h_0 = 150\text{--}250\text{ nm}$  onto a cleaned  $1\text{ cm}^2$  silicon substrate, as shown in Figure 1a, and subsequently treat the sample in an oxygen plasma for a few seconds to decrease the hydrophobicity of the polymer film. After charging the PMMA layer with PDDA solution, we deposit a droplet of water-suspended polystyrene (PS) spheres with 100 nm diameter on the sample (see Figure 1b). The PMMA layer is now covered with well separated PS spheres which are arranged in a random spatial fashion. Afterward, a thin oxygen plasma resistant film (5 nm Cr and 20 nm Au) is evaporated on top of the sample, as shown in Figure 1c, and then the PS spheres are removed. Finally, an isotropic oxygen plasma etching step creates extended holes in the PMMA layer underneath the holes in the gold mask (Figure 1d).

The hole-mask is then utilized for the fabrication of the split-ring-resonator metamaterial, which serves as resonant nanoantenna SEIRA substrate. As shown in Figure 1e, we evaporate gold to form the SRRs in a similar fashion as our previously described nanosphere lithography.<sup>13,14</sup> Figure 1f shows the lift-off process. The whole ( $1\text{ cm}^2$ ) sample is then covered with well separated, randomly placed SRR structures with unique orientation of their gaps.

Using this fabrication method, we can prepare nanostructures over even larger areas. The size of the sample is only limited by the fabricated homogeneous PMMA area using spin-coating. Using different fabrication settings such as azimuthal angle  $\theta$  and polar angle  $\varphi$  in combination with opening and closing the shutter and using different evaporation metals, we can control the various geometry and material parameters of the structures very precisely.

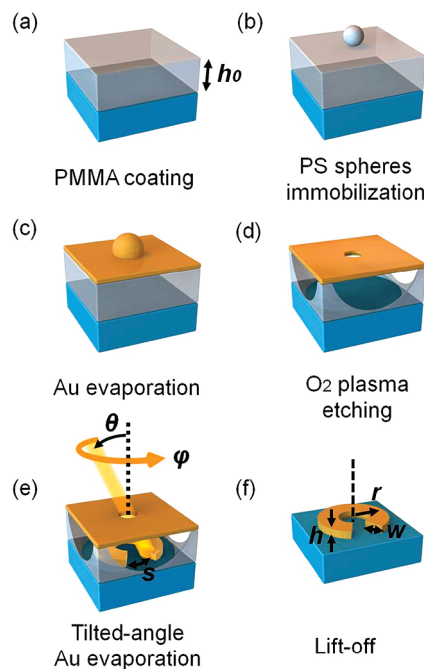


**Figure 1.** Fabrication scheme: (a) deposition of sacrificial PMMA layer; (b) deposition of polystyrene spheres in an arbitrarily distributed arrangement; (c) evaporation of oxygen plasma resistant Au-mask; (d) removing polystyrene spheres with ultrasonic bath and subsequent isotropic dry etching leads to extended holes in PMMA layer; (e) evaporation of the structures by tilted angle evaporation (polar rotation angle  $\varphi$ , azimuthal tilt angle  $\theta$ ); (f) lift-off of the sacrificial PMMA layer.

The resolution depends only on the size of the used nanospheres and can easily go down to a 50 nm metal line width and gap widths below 10 nm. The repeatability and reliability is extremely high, as inhomogeneous broadening factors are rather limited during our fabrication process.

The successful preparation of the metamaterial SRR nanoantennas is shown in Figure 2. The scanning electron microscopy (SEM) images of large area (Figure 2a,c) demonstrate the low defect concentration of our method. Larger magnification (Figure 2b,d) shows the SRR geometry details, the low inhomogeneous broadening, as well as the sufficient spacing between neighboring elements. Figure 2e shows an AFM image of a split-ring-resonator, and Figure 2f shows a height profile along a cross-section to obtain the maximum structure height of 25 nm.

To obtain the required field enhancement for SEIRA, we match the wavelength of the fundamental plasmon mode of the split-ring-resonators with the vibrational resonance of the molecule of interest. We simulate the required geometry parameters using an FDTD code (CST Microwave Studio). The refractive index of silicon is assumed to be  $n = 3.45$ , and the permittivity of bulk gold is described by a Drude model with plasma frequency  $\omega_p = 1.37 \times 10^{16}\text{ Hz}$  and a damping constant  $\kappa = 1.2 \times 10^{14}\text{ Hz}$ . The gap size, the inner and

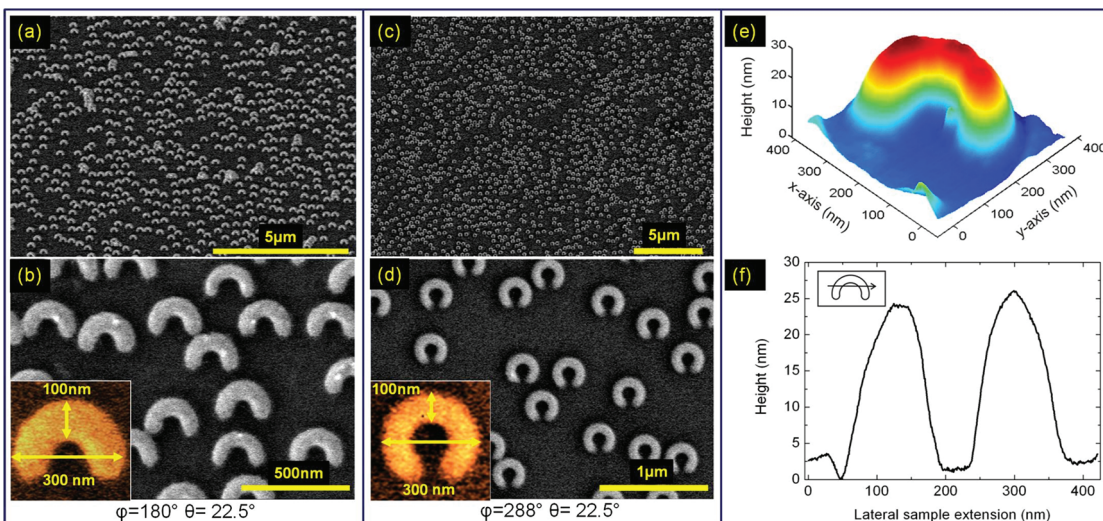


**Figure 2.** SEM images and AFM measurement of split-ring-resonators produced by hole-mask colloidal-lithography. (a,c) SEM overview showing homogeneous, random coverage over large areas for two types of split-ring resonators. (b,d) Split-ring resonators with 300 nm diameter, 100 nm gold width, and 25 nm gold thickness. The evaporation parameters are polar angle range  $\varphi = 180^\circ$  (b) or  $\varphi = 288^\circ$  (d) and azimuthal angle  $\theta = 22.5^\circ$ . The split-rings are mostly well separated from each other. (e) Three dimensional AFM image of a single split-ring-resonator with  $\varphi = 180^\circ$ . (f) Height profile of the split-ring-resonator in panel e along the cross-section line shown in the upper left corner. The top height is about 25 nm.

outer diameter, and the structure height are varied in order to adjust the desired resonance wavelength. The split-ring geometry allows for particularly easy tuning of the resonance wavelength by simply varying the gap opening angle. In comparison to linear antennas the resonance frequency of split-ring-resonators can be tuned without changing the area per split-ring-resonator.

Optical characterization of the manufactured structures was carried out using a Fourier-transform infrared (FTIR) spectrometer (Bruker Vertex-80) attached with an IR microscope (Bruker Hyperion II). Optical spectra were obtained using an MCT-detector for normally incident light polarization along and perpendicular to the SRR gap in reflectance geometry. The bare silicon substrate serves as reference. We plot relative reflectance on the y-axis which is larger than 1 as the background reflectance of silicon is only about 25% and the reflectance of the gold structures on the substrate is significantly higher. Figure 3a compares experimental results with FDTD simulations for polarization along the gap, and Figure 3b for polarization perpendicular to the gap, which show good agreement. Different spectral linewidths arise probably from residual inhomogeneous broadening from surface roughness, from deviations of the gold dielectric function, and due to interaction of neighboring split-rings. The fundamental (Figure 3a) and second-order plasmon resonance (Figure 3b) are clearly identified.

To demonstrate the SEIRA activity we covered the SRRs with one monolayer of ODT ( $\text{SH}(\text{CH}_2)_{17}\text{CH}_3$ ) and d-ODT ( $\text{SD}(\text{CD}_2)_{17}\text{CD}_3$ ), respectively. The preparation of the sample with ODT is described in detail in the Supporting Information. We choose ODT as the probe

molecule since its absorption characteristics on gold is known from the preparation of self-assembled monolayers<sup>15</sup> and was recently applied to cover nanoantennas for SEIRA.<sup>16</sup> Because of the specific binding of sulfur to gold, multilayer adsorption as well as adsorption on surfaces other than gold is inhibited. Furthermore, ODT features strong IR vibrational bands mainly provided by its  $\text{CH}_2$  groups, which are well suited for our SEIRA experiments with vibrational modes at  $2855 \text{ cm}^{-1}$  ( $\lambda = 3500 \text{ nm}$ ) and  $2927 \text{ cm}^{-1}$  ( $\lambda = 3420 \text{ nm}$ ). Inconveniently,  $\text{CH}_2$  groups are also present in organic residues, which for example may originate from the PMMA used during the fabrication process. To exclude such an unwanted contribution to the enhanced ODT signals and to demonstrate the easy adjustability of the SRRs in SEIRA, we also carried out experiments with d-ODT with vibrational modes at  $2089 \text{ cm}^{-1}$  ( $\lambda = 4790 \text{ nm}$ ) and  $2195 \text{ cm}^{-1}$  ( $\lambda = 4560 \text{ nm}$ ).<sup>17</sup>

Reflection spectra of SRRs with a polar evaporation angle of  $180^\circ$  before and after deposition of ODT are shown in Figure 4a,b, for IR radiation polarized parallel to the gap. In addition to the fundamental SRR resonance,  $\text{CH}_2$  vibrations at  $2855 \text{ cm}^{-1}$  ( $\lambda = 3500 \text{ nm}$ ) and  $2929 \text{ cm}^{-1}$  ( $\lambda = 3410 \text{ nm}$ ) (see inset) are observed after deposition of ODT. Since no  $\text{CH}_2$  vibrations are visible in the spectrum before ODT adsorption we conclude that the appearance of the molecular vibrations originates from the resonantly enhanced near-fields of the SRR excitation. This result also shows that no organic residues containing  $\text{CH}_2$  are remaining on the SRRs and therefore proves the success of  $\text{O}_2$  ashing. Measurements in perpendicular polarization show no enhanced signals after ODT deposition (Figure 4b), which proves

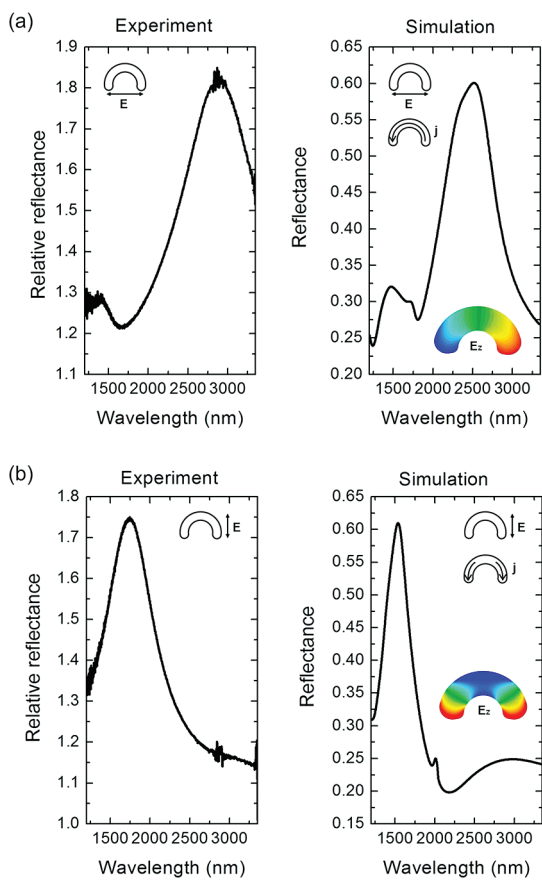


**Figure 3.** Experimental (FTIR) and numerically simulated (FDTD) reflectance spectra of the  $\varphi = 180^\circ$  split-ring-resonators. The experimental spectra are normalized with respect to the bare Si substrate. We plot relative reflectance on the y-axis which is larger than 1 as the background reflectance of silicon is only about 25% and the reflectance of the gold structures on the substrate is significantly higher. The left column shows the experimental results for polarization of the incident electric field linearly polarized parallel to the gap (a) and orthogonal to the gap (b). The right column shows the simulated spectra for both polarizations and the current flow  $j$  (cartoon) as well as the color coded (red = positive value, blue = negative value, same scale for both plots) electric field  $E_z$  (component perpendicular to structure) at the respective resonances.

that our ODT concentration is below the detection limit of standard IR spectroscopy. The signals are only resonantly enhanced if  $\omega_{\text{ODT}}$  roughly matches the far field resonance frequency  $\omega_{\text{res}}$ . As known from theoretical studies<sup>18,19</sup> the maximum near-field enhancement is expected at values slightly larger than  $\omega_{\text{ODT}}/\omega_{\text{res}} = 1$ . Thus the observed ODT signal can be further maximized by optimizing the SRR resonance with respect to the vibrational bands.

A better match is achieved for SRRs with a polar evaporation angle  $\varphi = 288^\circ$  covered with d-ODT, as shown in Figure 5. We define the polarization along the gap as  $0^\circ$ . Figure 5a shows the reflectance spectra of the SRRs before the deposition of d-ODT for different polarization. Choosing incident light polarization from  $0$  to  $90^\circ$ , one can select different metamaterial antenna

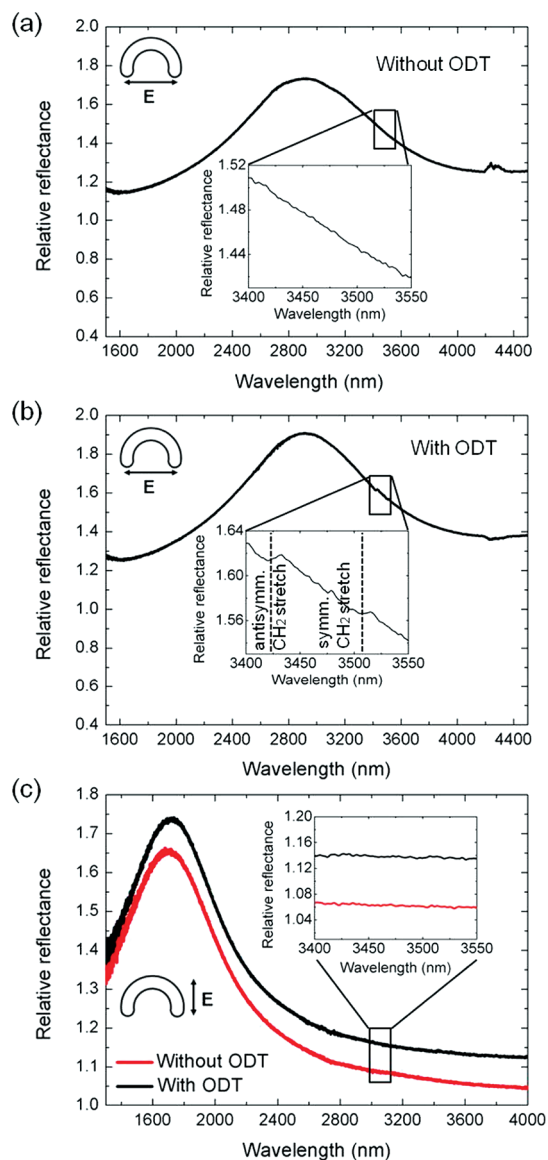


**Figure 4.** Utilization of split-ring-resonators from Figure 2a, b as SEIRA substrate. We show relative reflectance spectra with bare Si reflectance as reference: (a) without monolayer of ODT. Only the fundamental plasmon mode is visible for excitation along the gap; (b) with monolayer of ODT and light polarized along the gap, at  $2924 \text{ cm}^{-1}$  (3420 nm) and  $2849 \text{ cm}^{-1}$  (3510 nm), the antisymmetric and symmetric  $\text{CH}_2$ -stretch modes of ODT are visible as modulation of the reflectance spectra; (c) with light polarized perpendicular to the gap, the higher order plasmon mode at 1670 nm is excited. Hence no SEIRA enhancement of the ODT vibrational modes around 3400–3550 nm is visible.

resonance positions. In particular, a polarization of  $45^\circ$  exhibits three resonances throughout the near IR range. Therefore, our material is perfectly suitable for multiline resonantly enhanced SEIRA, as recently proposed.<sup>20,21</sup> Modifying the SRR geometry to an elliptical shape with suitably adjusted evaporation angles would give us even the freedom to independently tune the parallel *versus* the perpendicular resonances with respect to the gap.

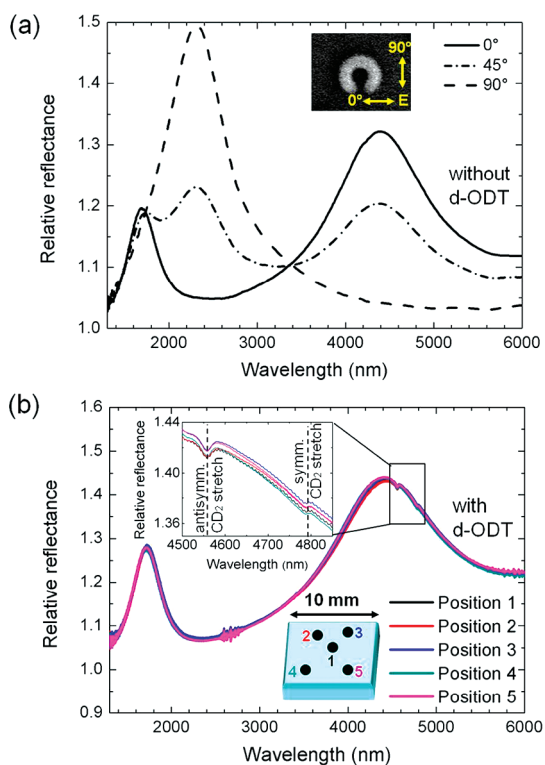


**Figure 5. Utilization of split-ring-resonators from Figure 2c, d as SEIRA substrate. We used the SRR fundamental plasmon mode around  $4.4\ \mu\text{m}$ .** (a) Spectra of structures before deuterated (d)-ODT deposition with linearly polarized light at angles  $0^\circ$ ,  $45^\circ$ , and  $90^\circ$  with respect to the gap, which is illustrated in the inset. Different split-ring resonances at around 1700, 2400, and 4400 nm can be excited. (b) Spectra of the structures after d-ODT deposition using linearly polarized light parallel to the gap. The different spectra are measured at different positions of the sample, which is illustrated in the cartoon in the lower right corner. All the spectra show the same plasmon excitation and the same d-ODT signal. This is a further proof for the homogeneity of the sample. The spectra in the upper left corner show the two strongest modes of d-ODT: antisymmetric  $\text{CD}_2$  stretch at  $2193\ \text{cm}^{-1}$  (4559 nm) and symmetric  $\text{CD}_2$  stretch at  $2086\ \text{cm}^{-1}$  (4793 nm).

Figure 5b shows the reflectance spectra after the deposition of d-ODT for the polarization  $0^\circ$ . Here the symmetric  $\text{CD}_2$  vibration is at  $2089\ \text{cm}^{-1}$  ( $\lambda = 4790\ \text{nm}$ ), and the antisymmetric  $\text{CD}_2$  vibration at  $2195\ \text{cm}^{-1}$  ( $\lambda = 4560\ \text{nm}$ ) nearly coincides with the fundamental SRR resonance. To verify the homogeneous distribution of SRRs and the low defect concentration on our sample we carried out laterally resolved IR spectroscopic measurements in addition to the aforementioned SEM analysis. A circular aperture with diameter of about  $100\ \mu\text{m}$  allows us to record relative reflectance spectra at different sample positions with separation distances in the millimeter range. As depicted in Figure 5b, the plasmonic response of the SRRs as well as the enhanced d-ODT signal is nearly identical for different positions on the sample. This fact confirms the extremely homogeneous large-area fabrication of SRRs using hole-mask colloidal nanolithography.

To perform a quantitative analysis we compared the enhanced signal strength to the estimated reflectance of a monolayer ODT (d-ODT) on a bare signal silicon wafer. Since the ODT (d-ODT) signal in such a configuration is below the noise level we estimated a signal from infrared reflection absorption spectroscopy (IRRAS) of one monolayer ODT (d-ODT) on a gold wafer. Using Fresnel equations for a three-layer system, as present in previous IRRAS studies,<sup>22</sup> we obtained signal strengths of about 0.0039% (antisymmetric  $\text{CH}_2$ ) and 0.0016% (symmetric  $\text{CH}_2$ ) for one monolayer ODT on silicon. For d-ODT we obtain 0.0026% (antisymmetric  $\text{CD}_2$ ) and 0.002% (symmetric  $\text{CD}_2$ ). To estimate enhancement factors we need to consider the relative fractions of the illuminated spot area effectively covered with molecules. While in IRRAS measurements the whole gold film is covered by ODT, only a small part of the illumination spot in SEIRA measurements is covered by molecules due to the selective adsorption on the gold SRRs. Further, due to the distribution of the electromagnetic near-field around the SRRs the enhanced molecular signal mainly originates from the ends of the SRRs. Considering both effects we estimate enhancement factors in our case up to 8000 for ODT covered SRRs and up to 20000 for d-ODT covered SRRs.

Compared to SEIRA measurements using linear antennas<sup>16,23</sup> lower enhancement factors are observed, which may be due to different crystalline quality as a result of different fabrication processes. Additionally, the surface roughness is expected to affect the SEIRA signal enhancement. This does not mean that a perfectly smooth surface yields the highest enhancement as for example known from SERS measurements. Also carbon deposited during SEM imaging, which is only partially removed by  $\text{O}_2$  ashing, may suppress ODT (d-ODT) adsorption. Also, a major factor for lower SEIRA enhancement is the high refractive index of the silicon substrate. This effect can be understood in analogy to propagating surface plasmons at metal-dielectric interfaces, where a larger portion of the electric field is squeezed into the metal for materials with higher dielectric constants.<sup>24</sup> This effect reduces the field that can interact with the ODT on top.  $\text{CaF}_2$  substrates will allow for enhancement factors as large as 500000.<sup>7</sup>

## CONCLUSIONS

We have demonstrated a low-cost and reliable method to fabricate a large-area of  $\text{cm}^2$  size with extremely homogeneous SRR metamaterials. We have furthermore proven their suitability for resonant antenna SEIRA enhancement up to 20000-fold. Also, multiparticle oligomer geometries,<sup>25–27</sup> as well as stacked and chiral geometries are possible with our new fabrication method. Our method will allow in the future, due to its ease of geometry variation, the fabrication of low-cost and homogeneous large-area Fano-resonant

asymmetric metamaterials<sup>20</sup> for plasmon-induced transparency assisted SEIRA. This should pave the road toward a whole new generation of low-cost high-efficiency infrared spectroscopy methods for pharmaceutical

drug screening and few-biomolecule detection with zeptomolar sensitivity, thus making resonant plasmon-enhanced spectroscopy a standard bio- and medical lab tool.

## METHODS

**Hole-Mask Fabrication.** We use a 380  $\mu\text{m}$  thick polished silicon substrate, which is cleaned with acetone and isopropanol in an ultrasonic bath for about 10 min and then dried using nitrogen. A 150–250 nm thick PMMA layer (Sigma Aldrich, 200k 4 wt % in chlorobenzene AR-P 641.04) is spin coated onto the silicon substrate and hard baked at 165 °C for 2 min. To decrease the hydrophobicity of the polymer film, we treat the sample in an oxygen plasma for 12 s (TECHNICS GMBH, PAV TePla 100-E, 250 mTorr, 50 W). We then immediately pipet a droplet of a polyelectrolyte solution (Sigma Aldrich, PDDA, 0.2 wt % in water) on top of the sample, to provide a net charge to the PMMA layer. This is followed by rinsing the sample with deionized water and drying in a nitrogen stream. After charging the layer, we deposit a droplet of water suspended polystyrene (PS) spheres (Polysciences, Polybead Microspheres 100 nm diameter, 0.02 wt % in water), which is ultrasonicated for 30 min, on the sample and rinse it away with deionized water after 1 min. In the next step, we put the sample into a hot water bath (98 °C, 3 min) and dry it with nitrogen. The PMMA layer is now covered with well separated PS spheres which are arranged in a random spatial fashion. Subsequently, a thin oxygen plasma resistant film (5 nm Cr and 20 nm Au) is evaporated on top of the sample. We used an ultrasonic bath with controllable power (90 V, 12 min) to remove the PS spheres afterward and obtained a perforated gold layer on top of the thick PMMA layer. Finally, an isotropic etching step (oxygen plasma, 7 min, 250 W, 1 Torr, same machine as above) creates extended holes in the PMMA layer underneath the holes in the gold mask. After the evaporation process, the sacrificial PMMA layer is removed by immersing the sample into 65 °C warm *N*-methyl-2-pyrrolidone (NMP) for 2 h, and the sample is then flushed with isopropanol.

**Evaporation of SRRs.** The evaporation process is carried out in a modified thermal evaporation machine (Edwards E306). The sample can be rotated inside the evaporation chamber in polar and azimuthal directions using two vacuum-compatible stepper motors. The control of the azimuthal angle  $\theta$  and the polar angle  $\varphi$  in combination with the PMMA thickness  $h_0$  determines the radius  $r$  and the gap size  $s$  of the SRRs, as shown in Figure 1e,f. The radius  $r$  is given by

$$r = h_0 \tan \theta \quad (1)$$

and the gap size  $s$  is determined by

$$s = 2\pi r \frac{360^\circ - \phi}{360^\circ} = 2\pi h_0 \tan \theta \frac{360^\circ - \phi}{360^\circ} \quad (2)$$

The width of the SRR  $w$  is determined by the mask-hole diameter, namely, the diameter of the used nanospheres. A layer thickness monitor (crystal oscillator) is used to determine the structure height  $h$ . First we evaporate a thin adhesion layer of chromium onto the silicon substrate and subsequently evaporate the gold. To calculate the obtained structure height  $h$  we use a geometrical model, which is explained in the Supporting Information, resulting in

$$h = h_1 \frac{45^\circ w}{\varphi h_0 \tan \theta} \quad (3)$$

Here  $h_1$  is the evaporated material thickness, which is displayed on the layer thickness monitor.

**Preparation with ODT.** After cleaning the SRRs with O<sub>2</sub> plasma ( $t = 30$  s, 1 Torr, 250 W) in order to remove organic residuals, we immersed the gold SRR supported by a Si Wafer in a 100  $\mu\text{molar}$  solution of ODT (Sigma Aldrich) in ethanol for eight hours. SRR

prepared on a different Si-wafer covered with d-ODT (provided by the Physical Chemical Institute, University Heidelberg) were immersed in a 20  $\mu\text{molar}$  solution of d-ODT in ethanol for at 24 h. During this time a selective adsorption of ODT (d-ODT, respectively) on gold SRRs took place. Afterward the samples were rinsed with ethanol and dried using nitrogen flow to remove nonspecifically bound ODT (d-ODT) molecules. As a result, samples with well-defined surface coverage (no molecules on Si, one monolayer on gold SRRs) are obtained, which is the precondition for a quantitative analysis of the SEIRA signals.

**Acknowledgment.** We acknowledge Dr. H. Fredriksson for his help for the hole-mask fabrication. We acknowledge Prof. Dr. H. Schweizer for discussions about nanofabrication. We acknowledge B. Fenk for his FIB cutting. We also acknowledge M. Uhl and H. Gräbeldinger for technical assistance. F. Neubrech acknowledges funding within the "Nanoantenna" collaborative European project (No. HEALTH-F5-2009-241818). This work was financially supported by DFG (FOR 730), BMBF (3D Metamat and Was-Sens), BW-Stiftung, and the Alexander von Humboldt foundation (Bessel Prize).

**Supporting Information Available:** The derivation of the expression for the SRR geometry parameters. This material is available free of charge via the Internet at <http://pubs.acs.org>.

## REFERENCES AND NOTES

- McFarland, A. D.; Young, M. A.; Dieringer, J. A.; Van Duyne, R. P. Wavelength-Scanned Surface-Enhanced Raman Excitation Spectroscopy. *J. Phys. Chem. B* **2005**, *109*, 11279–11285.
- Odom, T. W.; Nehl, C. L. How Gold Nanoparticles Have Stayed in the Light: The 3M's Principle. *ACS Nano* **2008**, *2*, 612–616.
- Nordlander, P. The Ring: A Leitmotif in Plasmonics. *ACS Nano* **2009**, *3*, 488–492.
- Hao, F.; Nordlander, P.; Sonnenaud, Y.; Van Dorpe, P.; Maier, S. A. Tunability of Subradiant Dipolar and Fano-Type Plasmon Resonances in Metallic Ring/Disk Cavities: Implications for Nanoscale Optical Sensing. *ACS Nano* **2009**, *3*, 643–652.
- Kundu, J.; Le, F.; Nordlander, P.; Halas, N. J. Surface Enhanced Infrared Absorption (SEIRA) Spectroscopy on Nanoshell Aggregate Substrates. *Chem. Phys. Lett.* **2008**, *452*, 115–119.
- Le, F.; Brandl, D. W.; Urzumov, Y. A.; Wang, H.; Kundu, J.; Halas, N. J.; Aizpurua, J.; Nordlander, P. Metallic Nanoparticle Arrays: A Common Substrate for Both Surface-Enhanced Raman Scattering and Surface-Enhanced Infrared Absorption. *ACS Nano* **2008**, *2*, 707–718.
- Neubrech, F.; Pucci, A.; Cornelius, T. W.; Karim, S.; Garcia-Etxarri, A.; Aizpurua, J. Resonant Plasmonic and Vibrational Coupling in a Tailored Nanoantenna for Infrared Detection. *Phys. Rev. Lett.* **2008**, *101*, 157403.
- Cubukcu, E.; Zhang, S.; Park, Y. S.; Bartal, G.; Zhang, X. Split Ring Resonator Sensors for Infrared Detection of Single Molecular Monolayers. *Appl. Phys. Lett.* **2009**, *95*, 043113.
- Prycet, I. M.; Kelaitat, Y. A.; Aydint, K.; Atwater, H. A. Compliant Metamaterials for Resonantly Enhanced Infrared Absorption Spectroscopy and Refractive Index Sensing. *ACS Nano* **2011**, *5*, 8167–8174.
- Lahiri, B.; Khokhar, A. Z.; De La Rue, R. M.; McMeekin, S. G.; Johnson, N. P. Asymmetric Split Ring Resonators for

- Optical Sensing of Organic Materials. *Opt. Express* **2009**, *17*, 1107–1115.
- 11. Lahiri, B.; McMeekin, S. G.; De La Rue, R. M.; Johnson, N. P. Resonance Hybridization in Nanoantenna Arrays Based on Asymmetric Split-Ring Resonators. *Appl. Phys. Lett.* **2011**, *98*, 153116.
  - 12. Fredriksson, H.; Alaverdyan, Y.; Dmitriev, A.; Langhammer, C.; Sutherland, D. S.; Zäch, M.; Kasemo, B. Hole-Mask Colloidal Lithography. *Adv. Mater.* **2007**, *19*, 4297–4302.
  - 13. Gwinnier, M. C.; Koroknay, E.; Fu, L. W.; Patoka, P.; Kandulski, W.; Giersig, M.; Giessen, H. Periodic Large-Area Metallic Split-Ring Resonator Metamaterial Fabrication Based on Shadow Nanosphere Lithography. *Small* **2009**, *5*, 400–406.
  - 14. Zhao, J.; Frank, B.; Burger, S.; Giessen, H. Large-Area High-Quality Plasmonic Oligomers Fabricated by Angle-Controlled Colloidal Nanolithography. *ACS Nano* **2011**, *5*, 9009–9016.
  - 15. Schreiber, F. Structure and Growth of Self-Assembling Monolayers. *Prog. Surf. Sci.* **2000**, *65*, 151–257.
  - 16. Neubrech, F.; Kolb, T.; Lovrincic, R.; Fahsold, G.; Pucci, A.; Aizpurua, J.; Cornelius, T. W.; Toimil-Molares, M. E.; Neumann, R.; Karim, S. Resonances of Individual Metal Nanowires in the Infrared. *Appl. Phys. Lett.* **2006**, *89*, 253104.
  - 17. Yang, S.-C.; Richter, L. J.; Stephenson, J. C.; Briggman, K. A. *In Situ*, Vibrationally Resonant Sum Frequency Spectroscopy Study of the Self-Assembly of Dioctadecyl Disulfide on Gold. *Langmuir* **2002**, *18*, 7549–7556.
  - 18. Aizpurua, J.; Bryant, G. W.; Richter, L. J.; Garcia de Abajo, F. J.; Kelley, B. K.; Mallouk, T. Optical Properties of Coupled Metallic Nanorods for Field-Enhanced Spectroscopy. *Phys. Rev. B* **2005**, *71*, 235420.
  - 19. Zuloaga, J.; Nordlander, P. On the Energy Shift between Near-Field and Far-Field Peak Intensities in Localized Plasmon Systems. *Nano Lett.* **2011**, *11*, 1280–1283.
  - 20. Wu, C.; Khanikaev, A. B.; Adato, R.; Arju, N.; Yanik, A. A.; Altug, H.; Shvets, G. Fano-Resonant Asymmetric Metamaterials for Ultrasensitive Spectroscopy and Identification of Molecular Monolayers. *Nat. Mater.* **2011**, *10*.1038/nmat3161.
  - 21. Liu, N.; Tang, M. L.; Hentschel, M.; Giessen, H.; Alivisatos, A. P. Nanoantenna-Enhanced Gas Sensing in a Single Tailored Nanofocus. *Nat. Mater.* **2011**, *10*, 631–636.
  - 22. Enders, D.; Pucci, A. Surface Enhanced Infrared Absorption of Octadecanethiol on Wet-Chemically Prepared Au Nanoparticle Films. *Appl. Phys. Lett.* **2006**, *88*, 184104.
  - 23. Adato, R.; Yanik, A. A.; Amsden, J. J.; Kaplan, D. L.; Omenetto, F. G.; Hong, M. K.; Erramilli, S.; Altug, H. Ultrasensitive Vibrational Spectroscopy of Protein Monolayers with Plasmonic Nanoantenna Arrays. *Proc. Natl. Acad. Sci. U.S.A.* **2009**, *106*, 19227–19232.
  - 24. Raether, H. *Surface Plasmons*; Springer-Verlag: Berlin, 1986; pp 6.
  - 25. Lassiter, J. B.; Sobhani, H.; Fan, J. A.; Kundu, J.; Capasso, F.; Nordlander, P.; Halas, N. J. Fano Resonances in Plasmonic Nanoclusters: Geometrical and Chemical Tunability. *Nano Lett.* **2010**, *10*, 3184–3189.
  - 26. Hentschel, M.; Dregely, D.; Vogelgesang, R.; Giessen, H.; Liu, N. Plasmonic Oligomers: The Role of Individual Particles in Collective Behavior. *ACS Nano* **2011**, *5*, 2042–2050.
  - 27. Dregely, D.; Hentschel, M.; Giessen, H. Excitation and Tuning of Higher-Order Fano Resonances in Plasmonic Oligomer Clusters. *ACS Nano* **2011**, *5*, 8202–8211.